

This technical paper was written and developed in October, 2001 when the author(s) was an employee of Dyneon LLC. Dyneon LLC was formerly a wholly-owned subsidiary of 3M Company and was fully integrated into 3M Company on January 1, 2011.

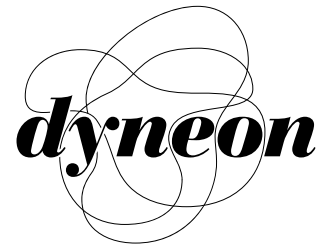
Title:

Visualizing the elimination of sharkskin through polymer processing additives (PPAs): Coating and polymer-polymer slippage

Synopsis:

We developed a capillary rheo-optics technique to visualize how fluoropolymer polymer processing additives (PPAs) eliminate a surface distortion called “sharkskin” in the extrudate of linear low-density polyethylene (LLDPE). The measurements were carried out in a transparent sapphire tube located at the exit of a twin-screw extruder. Depth-resolved optical microscopy was used to measure both the polymer velocity profiles and to image the coating process of the PPA onto the capillary wall. In the absence of PPA, no slippage occurs between the capillary wall and the polyethylene; sharkskin was observed at all flow rates. Upon addition of the PPA to the LLDPE, the PPA migrates to the capillary wall where it sticks and induces slippage between itself and the LLDPE, concomitant with the elimination of sharkskin. The interface between the PPA and LLDPE is characterized by long stripes in the flow direction. Large values of the polymer-polymer slippage parameter were found which indicate that the fluoropolymer and LLDPE are fully disentangled at their interface. The PPA acts by dramatically reducing the extensional deformation of the LLDPE at the exit surface.

Date Published: October, 2001



*A 3M Company*

**Visualizing the elimination of sharkskin  
through polymer processing additives (PPAs):  
Coating and polymer-polymer slippage**

K. B. Migler  
Polymer Division, NIST

C. Lavallée  
3M Canada

M. P. Dillon  
Dyneon LLC

S. S. Woods  
Dyneon LLC

C. L. Gettinger  
3M

## Synopsis

We developed a capillary rheo-optics technique to visualize how fluoropolymer polymer processing additives (PPAs) eliminate a surface distortion called “sharkskin” in the extrudate of linear low-density polyethylene (LLDPE). The measurements were carried out in a transparent sapphire tube located at the exit of a twin-screw extruder. Depth-resolved optical microscopy was used to measure both the polymer velocity profiles and to image the coating process of the PPA onto the capillary wall. In the absence of PPA, no slippage occurs between the capillary wall and the polyethylene; sharkskin was observed at all flow rates. Upon addition of the PPA to the LLDPE, the PPA migrates to the capillary wall where it sticks and induces slippage between itself and the LLDPE, concomitant with the elimination of sharkskin. The interface between the PPA and LLDPE is characterized by long stripes in the flow direction. Large values of the polymer–polymer slippage parameter were found which indicate that the fluoropolymer and LLDPE are fully disentangled at their interface. The PPA acts by dramatically reducing the extensional deformation of the LLDPE at the exit surface.

## INTRODUCTION

The throughput of several industrially important classes of polymers is limited by a processing defect known as “sharkskin,” which is a surface defect on the extruded polymer. The surface of the polymer becomes rough, resulting in a loss of gloss and a change in certain surface properties. Sharkskin occurs beyond a critical throughput and affects extrusion operations such as film blowing, film casting, extrusion blown molding, tube extrusion, and wire coating.

The situation has become more critical in recent years with the increasing use of linear low-density polyethylenes (LLDPE) and metallocene linear low-density polyethylene (mLLDPE). These materials are desirable for their good mechanical properties, but flow instabilities such as sharkskin occur which can limit their processability.<sup>20</sup> A substantial effort to understand and overcome sharkskin has been underway since it was first reported over 40 years ago.<sup>21</sup>

In the 1960s, the accidental discovery that sharkskin could be reduced or eliminated by the incorporation of a PPA allowed processors to increase throughput, reduce energy consumption, and enhance processing quality.<sup>2</sup> Since then, the use of fluoropolymer PPAs has become widespread in polyolefins; in fact, resin manufacturers often add it to their polymer resins as part of an additive package. Fluoropolymer additives migrate to the die surface during extrusion where they lower the surface energy, allowing the main polyolefin to slip at the wall<sup>2</sup>.

However, the study of polymer processing additives is made difficult for two reasons. First, there are no available in situ measurement tools. Thus, it is difficult to know whether a given additive migrates to the surface, and if so, does it induce slippage? Second, at a fundamental level the cause of sharkskin and the precise reason that fluoropolymer additives reduce it are still under debate. This lack of understanding of the mechanism makes it conceptually difficult to rationally design new materials.

In this work, we describe a capillary rheo-optics instrument that uses stroboscopic optical microscopy to complement the long-standing rheological studies. The optical microscope is used to conduct particle tracking velocimetry and to directly image the coating of the fluoropolymer onto the capillary wall. The results indicate that the fluoropolymer and the polyethylene are fully disentangled at their interface, causing slippage. This slippage then decreases the extensional deformation at the exit of the die, thus reducing sharkskin.

## REVIEW

There have been several reported causes of sharkskin as recently reviewed by Denn.<sup>12</sup> One idea is that sharkskin is caused by slippage in the die.<sup>35</sup> This conclusion is drawn in part by a change in slope that occurs when one plots the pressure drop across a capillary die as a function of throughput (i.e., mass flow). These conclusions are contradicted by results showing that sharkskin occurs without large-scale slip.<sup>11,14,23</sup>

Much evidence has accumulated which implicates the exit of the capillary as the site where sharkskin initiates. However, the mechanism is still under vigorous debate. Flow birefringence measurements at the exit region confirm the existence of a region of high stress at the exit of the capillary tube.<sup>4,14,15,27,34</sup> The polymer at (and near) the surface undergoes extreme stretching as the velocity goes from approximately zero in the region just before the tip of the capillary die to the extrudate’s final value just past the tip of the capillary tube. Above a critical tensile stress, the polymer ruptures at this free surface.<sup>10</sup> Inn et al.<sup>22</sup> were motivated by video imaging of polybutadiene extrusion to extend the Cogswell argument. Tremblay<sup>36</sup> based on numerical analysis work, suggested that cavitation at the die exit was at the origin of the sharkskin formation. This was correlated with experimental measurements on polydimethylsiloxane (PDMS). Wang and co-workers argue instead that sharkskin stems from an oscillating slip–stick transition that occurs due to an oscillating coil–stretch transition of the polymers adsorbed onto the capillary wall right at the exit.<sup>3</sup>

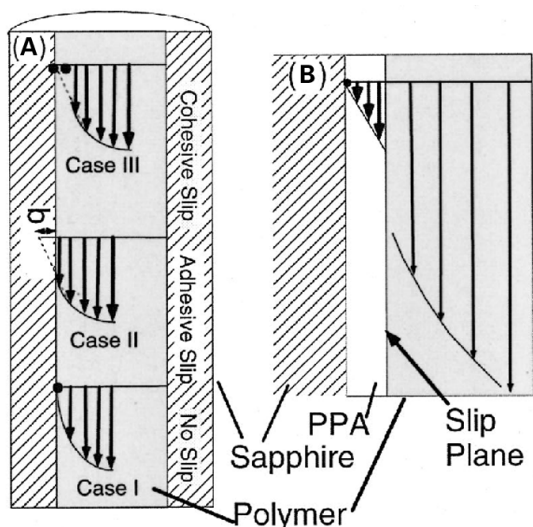


**FIG. 1. (A) Possible boundary conditions at the wall–polymer interface. Case I, standard no-slip approximation; case II, slippage occurs at the wall–polymer interface; and case III, a finite layer of polymer is stuck to the wall and slippage occurs in the polymer just beyond this layer. (B) In the case of a fluoropolymer preferentially wetting the wall, slippage may occur at the polymer–polymer interface.**

It is well known that the boundary conditions between the wall and the polymer can affect sharkskin. Changing the die to brass has been shown to reduce sharkskin and increase output at a given pressure in polyethylene.<sup>16,35</sup> Treating the die with a fluoropolymer has a similar, but more pronounced effect.

The use of a fluoropolymer as a processing aid is particularly interesting in that it represents the technologically most important example of polymer–polymer slippage. Experimentally, polymer–polymer slip has been indirectly observed by rheology in multilayers of polymer films.<sup>26</sup> In a fluoropolymer/PE system the rheological data of Hatzikiriakos and Dealy<sup>18</sup> can be interpreted as polymer–polymer slippage. In all these experiments, one observes reduced viscosities in the systems with interfaces. The topic of polymer–polymer slippage has also been treated theoretically.<sup>1,5,7,17</sup> Conceptually, one envisions the interface between two polymers as a region where the entanglement density is reduced compared to the bulk levels due to their incompatibility. The degree of incompatibility between the polymer pair determines the interpenetration of one polymer into the other, which is then related to the entanglement density at the interface. Since the viscosity is dominated by entanglement effects, the viscosity in the interfacial region is reduced. This reduced viscosity that occurs over a spatially thin region appears to the experimentalist as slip.

The boundary condition between the wall and the polymer melt is thus crucial to extrusion. Three general cases have been discussed in the literature, as shown in Fig. 1. In case I, we have the no-slip approximation. In case II, slippage occurs at the wall–polymer interface, known as adhesive slip. In case III, there is a finite layer of polymers stuck to the wall but there is an internal slip zone due to the high shear stress. This is known as cohesive slip. We also show one model [Fig. 1(B)] for what may happen in the case of a fluoropolymer additive in which the additive sticks to the wall but the polyethylene slips on the fluoropolymer. Spectroscopic technologies have shown a 5–15  $\mu\text{m}$  fluoropolymer layer coated on the internal die surface with a much smaller concentration on the extrudate<sup>9,25,33</sup> in support of the model in Fig. 1(B).

In order to distinguish between the three general cases described above, methodologies that complement the pressure/flow rheology must be utilized. Optical-based measurements can provide clean measurements of slip in polymer melts. Migler<sup>29</sup> utilized a fluorescence-based evanescent technique to document that slippage of a PDMS on a treated surface occurs within the first 100 nm of a solid (quartz) wall. That work also showed that slippage in the high shear regime can be ascertained by measuring that the bulk velocity profile does not extrapolate to zero at the wall. Laser-Doppler velocimetry was successful in measuring slippage of a high-density polyethylene during extrusion through a steel capillary slit, and mapped out interesting flow behavior during stick–slip.<sup>32</sup> The relationship between slippage and the surface conditions has been shown by various optical techniques.<sup>13,28,29,34</sup> Stroboscopic optical microscopy was utilized to monitor the flow profiles, as discussed below and preliminary evidence for slippage was found upon addition of a fluoropolymer additive to polyethylene.<sup>24,30,31</sup> Notably, Inn et al<sup>23</sup> found evidence of a stick boundary condition in the die land during sharkskin in polyisobutylene (PIB).

## EXPERIMENT

Many optical-based experiments utilize model systems such as PDMS or PIB because they are room-temperature melts and exhibit the sharkskin instability at relatively large time and length scales, making them amenable to experimental investigation. However, the driving force behind these model studies is the substantial economic consequences of the flow instabilities in polyethylene. The sharkskin instability occurs at high frequency, short wavelength, and of course, at elevated temperatures. Thus, few optical studies have been conducted on the behavior of PE in the sharkskin regime.<sup>27</sup> We show here that optical measurements are feasible by combining a simple sapphire flow cell with stroboscopic microscopy.

In this study, we utilize stroboscopic optical microscopy to visualize the mLLDPE/fluoropolymer systems as they are

extruded through a transparent circular capillary die. We utilize the microscope for two purposes. First, we make velocimetry measurements using a simple stroboscopic technique. Second, we directly image the polymer–polymer interface, thus gaining information about its structure and kinetics. The overall schematic is shown in Fig. 2. The heart of the system is the sapphire capillary tube, provided by Saphikon. (Certain commercial equipment, instruments, or materials are identified in this paper in order to adequately specify the experimental conditions. Such identification does not imply recommendation by the National Institute of Standards and Technology, Dyneon or 3M, nor does it imply that the materials are necessarily the best available for the purpose.) Sapphire is an excellent material because it is transparent from near UV to near IR, its thermal conductivity is near that of steel, and it withstands pressure well. The tube is grown as a single crystal. The surface of the inner circumference is not perfectly round, although this deviation is not believed to be serious. There are voids in the sapphire just below the inner surface which are visible in the optical microscope. The optic axis is perpendicular to (and intersects) the central tube axis. One end of the sapphire is inserted into a compression-sealing gland from Conax. This compression gland is composed of a soft graphite-composite material that seals the sapphire without breaking it. The other end of the sapphire is open to the atmosphere. The sealing gland screws into an attachment for a Haake capillary die, through a home-built coupler. The sapphire tubing is available in several diameters and is cut to whatever final length is desired. In this experiment the length of the tube is  $L=25.4$  mm and the radius is  $R=0.80$  mm. Interchanging sapphire tubes is a simple task; thus, experiments at various  $L/D$  ratios are possible. Thus far, we have not encountered any leakage, nor have we broken any sapphire capillary tubes. A capillary sapphire-based technology was developed by Brooks et al.<sup>8</sup> for contamination testing.

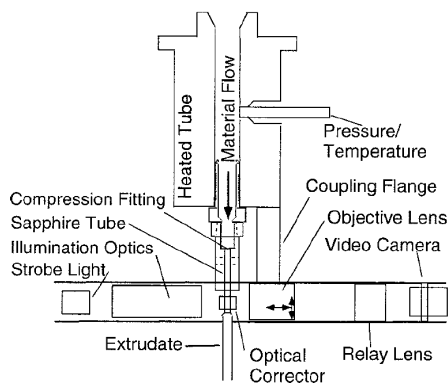


**FIG. 2. Schematic of the capillary rheo-optics apparatus in imaging mode. Molten polymer under pressure is extruded through the transparent sapphire tube. A stroboscopic optical microscope (comprised of the light source, illumination optics, objective lens and camera) produces depth-resolved images of the material as it flows through the capillary tube.**

We utilize stroboscopic optical microscopy for imaging the polymer under flow. This technique has been described in more detail in the case of a slit die.<sup>24</sup> For velocimetry measurements, we record video data from a standard charge-coupled-device camera onto a standard S-VHS video recorder. The stroboscopic light source is synchronized to flash twice per video frame; the time between flashes is controlled by the user and typically varies between 1 and 5 ms. Using an optical field of view of approximately 400  $\mu\text{m}$ , we obtain an upper velocity limit of about 400  $\mu\text{m/s}$ . While this velocity is sufficient for the current experiment, it could be increased by decreasing the time between flashes. For sufficiently low velocities the double strobe technique does not work, so we simply monitor how many video frames it takes for a particle to move a set distance—there is no lower limit on velocity. The depth of field  $D$  is a crucial parameter in this experiment. It is a function of the size of the particle being observed. Thus, large particles are in focus over a greater depth than are small ones. For smaller particles, the depth of field is approximately  $D = 50$   $\mu\text{m}$ , determined by monitoring the image of stationary small particles while translating the objective lens. In performing velocimetry measurements, care must be taken to measure small particles ( $\approx 2$   $\mu\text{m}$ ) or else the error in the depth of that particle will be too large. In this experiment, the “particles” are the naturally occurring gels, dust particles, and miscellaneous foreign objects that have found their way into the extruder. These need only be present in very small quantities to make measurements feasible.

The second use of the stroboscopic microscope is for imaging of polymer blend structure as documented in previous work using the optical slit die.<sup>19,24,30,31</sup> In the present case, it is used to observe the structure of the fluoropolymer/mLLDPE interface at the wall. The strobe light is necessary for imaging fast flowing objects, as well as for minimizing loss of clarity due to system vibration.

The curvature of the outer diameter of the sapphire tube causes spherical aberrations in the optical image. The solution is to slide a polished (on two sides) sapphire cube with a polished hole drilled through its center, over the sapphire tube. PDMS is placed in the narrow gap between the tube and the cube’s sleeve to minimize the index of refraction difference that would otherwise be caused if air filled that gap. Distortions due to the rounded sapphire/polymer interface are not serious when imaging near the optic axis. The capillary rheo-optics apparatus is situated at the exit of a Haake torque rheometer with a co-rotating twin-screw extruder attachment. The extruder melts, mixes, and then pumps the polymer through the capillary die. It could equally well be placed at the exit of a piston-based capillary rheometer.

## MATERIALS

The tests were carried out using a well-stabilized commercially available polyolefin mLLDPE [AFFINITY (trademark of The Dow Chemical Company) EG 8100 Polyolefin Plastomer]. It is

characterized by a melt index of 1.0, a density of 0.870 g/cm<sup>3</sup>, and contains some long-chain branching. This material was selected for its clarity, its overall low level of additives, and the absence of PPA in its formulation.

The processing additive used in this study was a commercially available copolymer of hexafluoropropylene and vinylidene fluoride (Dynamar™ PPA FX 9613). A commercially available master batch at a mass fraction of 3% PPA in a 2.0 MI LLDPE (Ampacet) was used. The master batch was tumble blended with the mLLDPE to achieve a mass fraction of PPA of 0.1%. Before the test, the equipment was purged using a commercially available purge compound (HM-10, Heritage Plastics) comprising a mass fraction of 70% CaCO<sub>3</sub> in a 10 MI LDPE.

## PROCEDURE

The goal of the experiment is to visualize how the fluoropolymer additive gets to the die surface and what it does once it gets there. The first component of the experiment is to study the system and velocimetry in the absence of the fluoropolymer. We carry out a series of five extrusions at increasing throughput. We utilize the twin-screw extruder in starve-feed mode in which pellets are fed into the twin-screw feed port at a controlled rate by a metering screw. The feed rate/RPM ratio is maintained constant as the throughput is increased so that the barrel of the twin screw maintains the same approximate fill ratio. (RPM is the rotations per minute of the twin screw.) There are three heating zones in the twin screw which are set (from feed to exit) at 130, 150, and 210 °C and the set point in the capillary die is 210 °C. In this experiment, we monitor flow rate, RPM, pressure at the die entrance, and screw torque. For each throughput, we conduct flow velocimetry measurements using the techniques described previously.

The extruder barrel was then cleaned by running an abrasive purge compound through it for approximately 2 h. For this procedure, the sapphire tube was replaced with a traditional rod die. Next, the pure resin without fluoropolymer additive was run through the extruder in order to remove the purge compound. When the extrudate finally became clear again, the sapphire tube was returned to the extruder.

In order to visualize how the PPA coats the die surface, we recorded the dynamics at the surface upon addition of PPA to the resin. After the system reached steady-state behavior, the velocimetry experiments were carried out under the same conditions (feed rate and temperature set points) as described previously in the case before the PPA was added.

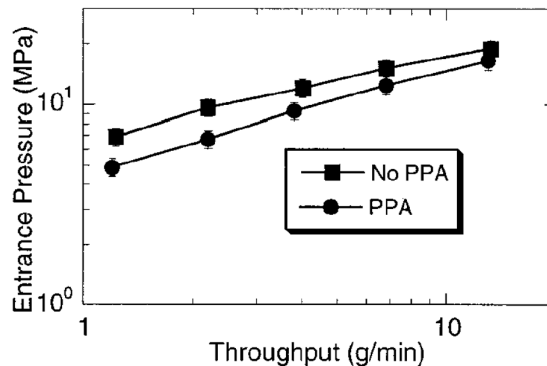


**FIG. 3. Entrance pressure of the metallocene linear low-density polyethylene (mLLDPE) as a function of throughput in the case of pure mLLDPE (no PPA), and in the case of mLLDPE with 1000 ppm fluoropolymer added as a polymer process additive (PPA).**

## RESULTS

Figure 3 shows a plot of the entrance pressure versus the mass throughput  $Q$ . The (uncorrected) wall shear stress is given by

$$\sigma_w = \frac{RP_c}{2L}, \quad (1)$$

where  $P_c$  is the pressure upstream of the capillary die, and  $R$  and  $L$  are the capillary radius and length, respectively. The standard deviation is shown and is due to pressure fluctuations. This is typical of the raw data that one obtains in a standard capillary experiment. It is clear that the fluoropolymer additive has a significant effect on the extrusion; for a given throughput, the pressure across the capillary die is reduced in all cases upon addition of the PPA. Note that the difference between the two curves narrows at the highest throughputs.

Sharkskin is observed for all throughputs in the absence of PPA. It is a strongly increasing function of throughput. At the lowest throughput, it is barely discernable under a microscope, whereas at the highest throughput it is easily seen with the unaided eye. Figure 4 shows a micrograph of the cooled extrudate in the absence of PPA at the highest throughput. In the case of the PPA, there is a complete disappearance of sharkskin.

Velocimetry results in the absence of PPA are shown in Fig. 5. The velocity profiles are taken from the center ( $r = 0$ ) to the wall ( $r = R$ ) where  $r$  is the radial distance from the center and  $R$  is the radius of the capillary ( $R = 0.8$  mm). The solid curves are fits obtained by using a power-law model for the viscosity:

$$V(r) = V_s + V_0[1 - (r/R)^{1+1/n}], \quad (2)$$

where  $V_s$  is the velocity at the surface  $V_s = V(R)$ ,  $V_0$  is the velocity at the center  $V_0 = V(0)$ , and  $n$  is the power-law index. In the fits,  $V_s$ ,  $V_0$ , and  $n$  are allowed to vary. On a linear scale, it appears that all curves converge to the no-slip condition  $V_s = 0$ .

In the actual measurement, any finite-sized particle in the immediate vicinity of the wall necessarily feels a force in the direction of flow and will move in that direction, as discussed below. Furthermore, because our depth of focus is approximately  $D = 50 \mu\text{m}$ , we measure a range of velocities in the near-surface region, from particles very near the wall whose velocities are  $V = \gamma e$  (where  $e \approx 1 \mu\text{m}$  is the radius of the smallest measurable particle) to those near the edge of the depth of focus  $V = \gamma D$ . For the plot of Fig. 5, the data point near the wall at  $r = 0.80 \text{ mm}$  corresponds to the smallest velocity that was measured. However, we do observe a continuous range of velocities at this point. This behavior will be seen to contrast with the velocity in the case of PPA. The typical standard deviations are shown in Fig. 5 for a throughput of  $6.8 \text{ g/min}$ . The error in the radial direction is due to the finite depth of field,  $D$ , and the relative standard deviation of the velocities is 5%, and applies to all the velocity profile curves in this paper. The resulting fitting parameters are shown in Table I.

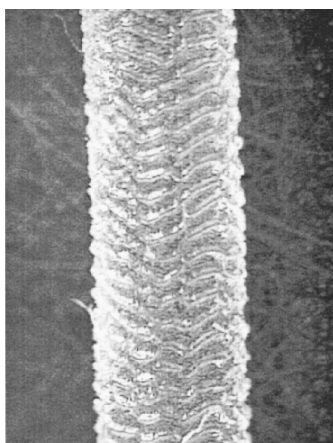


**FIG. 4. Micrographs of a cooled sample after extrusion without PPA. Height of the micrograph corresponds to 6.0 mm.**

After the extruder was purged and then flushed with pure mLLDPE, the resin with the PPA was added to the extruder. One goal of these experiments was to study how the PPA behaves when initially introduced into the extruder. The throughput was set to  $7.0 \text{ g/min}$  for which sharkskin is easily observable by the unaided eye. Figure 6 shows a plot of the evolution of the entrance pressure and the screw torque after the addition of the PPA. Initially, we extrude mLLDPE without the PPA. The standard deviation of the fluctuations is 5%.

At  $t = -350 \text{ s}$ , we stopped feeding the mLLDPE pellets while maintaining a constant RPM, so that the torque and pressure decrease as the quantity of material in the barrel decreases (first dashed line). At  $t = 0 \text{ s}$ , we added the mLLDPE plus PPA to the feed hopper, and the torque and shear stress quickly increase again. The video microscopy shows an interesting phenomenon at the surface of the die during the coat-on process. At approximately  $1000 \text{ s}$ , we observe gel-like

particles at the wall. These particles move in a jerky fashion; at times a given particle may stick to the wall, then it may move slowly, and at times it moves quickly. Figure 7 shows five gel particles at the wall. In time ( $\approx 10 \text{ s}$ ), these particles will move downstream and out of view. This micrograph is somewhat unusual in that the number of gel particles of this size is large. More typically, perhaps one gel particle in the  $20 \mu\text{m}$  size range is observed at a time, other gel particles are smaller. Once the coating is established, these gel-like particles are not visible or do not adhere to the die.

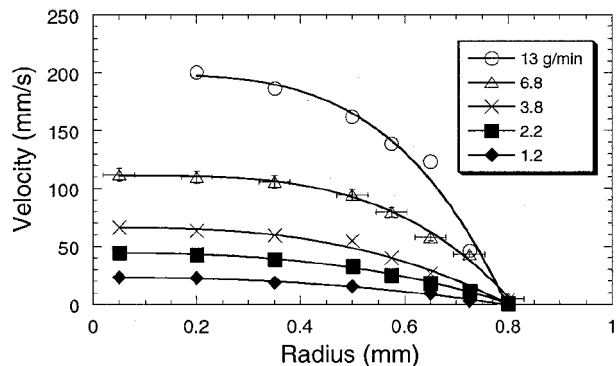


**FIG. 5. Velocity profiles obtained through direct imaging for the case of the pure mLLDPE (no PPA). These five flow rates correspond to those in the upper curve of Fig. 3. Data is obtained from the center of the capillary ( $r = 0.00 \text{ mm}$ ) to the bottom wall ( $r = 0.80 \text{ mm}$ ). The curves are best fits to a three-parameter power-law model with slippage [Eq. (2)]. At the wall,  $V=0 \text{ mm/s}$ , indicating that slippage is absent (or completely negligible) in these profiles.**

**TABLE I. Parameters and their standard deviation, obtained by fitting the measured velocity profiles to Eq. (2).**

	1 g/min	2 g/min	4 g/min	7 g/min	13 g/min	PPA?
$V_s$ (mm/s)	$-0.4 \pm 0.8$	$1.0 \pm 0.8$	$0 \pm 3$	$6 \pm 6$	$-3 \pm 10$	No
$V_0$ (mm/s)	$9.2 \pm 0.4$	$15.0 \pm 0.6$	$23.7 \pm 0.6$	$41.4 \pm 4$	$64 \pm 8$	Yes
$V_0$ (mm/s)	$24 \pm 1$	$43.5 \pm 1$	$66 \pm 3$	$104 \pm 3$	$201 \pm 10$	No
$V_0$ (mm/s)	$10.8 \pm 0.5$	$19 \pm 1$	$34.5 \pm 1$	$63 \pm 5$	$117 \pm 10$	Yes
$n$	$0.8 \pm 0.2$	$0.64 \pm 0.1$	$0.5 \pm 0.1$	$0.37 \pm 0.1$	$0.36 \pm 0.1$	No
$n$	$1.2 \pm 0.4$	$0.8 \pm 0.2$	$0.8 \pm 0.1$	$0.75 \pm 0.4$	$0.35 \pm 0.1$	Yes

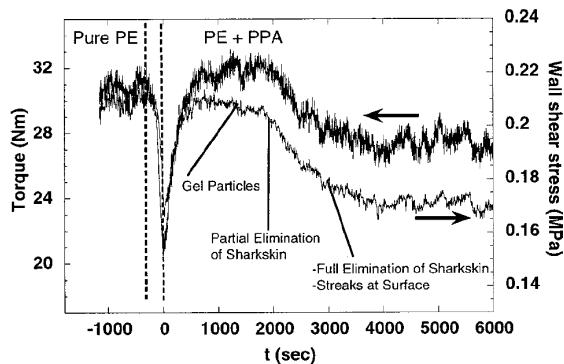


**FIG. 6. Evolution of the pressure and torque in the extruder system upon addition of the polymer processing**

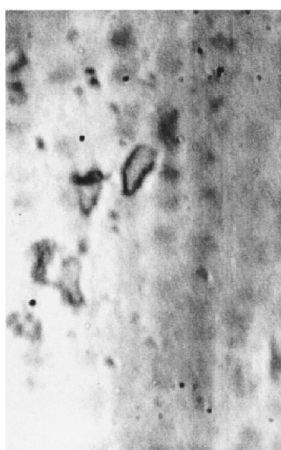


**FIG. 7. Micrograph of several slow moving/stuck gel particles that are observed 1300 s after the addition of the fluoropolymer additive. The height of the micrograph corresponds to 200  $\mu\text{m}$ .**

While we have not made a positive identification of these particles, it is known that PPA will clean a dirty extruder, releasing the accumulated degraded materials from the metal surfaces from the inside of the extruder.<sup>2</sup> It is also known that the PPA will prevent the formation of oxidized gels by presumably coating the die metal and preventing stagnation of the PE against the metal, therefore, preventing degradation.<sup>37</sup> Thus, it is likely that the gel particles are products of the cleaning of the die and barrel by the PPA.

At  $t = 1800$  s, we see a clear decrease in the levels of torque and shear stress. This steady decline continues until a new steady state is reached at  $t = 4200$  s. The wall shear stress and the torque experience relative

decreases of approximately 15% and 12%, respectively. We start to see a reduction in sharkskin at  $t = 2000$  s and by  $t = 3000$  s, it is eliminated—the surface is smooth. Concurrently, at  $t = 3000$  s, we begin to see a new phenomenon, the formation of streaks at the surface. At first, these streaks are difficult to discern, but their contrast increases as time proceeds. In Fig. 8 we show a micrograph taken at  $t = 10^4$  s, showing the streak phenomenon. The order of magnitude wavelength of the streaks is 5 mm. Observations of the dynamics of the streaks indicate that they are not static; we can observe their creation (streaks have been observed to “grow” down-stream) and their dissipation. Clearly, the streaks are due to the structure of the fluoropolymer at the surface. However, the cause of the streaking is not known at

this time. Possibilities include that individual PPA droplets hit the surface, stick and elongate in a streak, smearing on the surface as a lipstick. Alternatively, solid particles, such as the talc, could be creating scratch marks in the fluoropolymer layer. Finally, there may be a flow instability at the PPA/mLLDPE interface, causing the streak pattern. In any case, their appearance indicates the formation of the fluoropolymer layer with the concomitant elimination of sharkskin.

After the die is coated with PPA, the velocimetry indicates a significant difference in the behavior at the wall. We now observe two populations of particles near the surface within the depth of view of the microscope, one moving much faster than the other. Both populations do contain a spread of velocities but they are well separated and there is no overlap between them. In Fig. 9(A), we include both the fast and slow populations at the wall, the slow one being at  $V_S \approx 0$  mm/s and the fast one being at  $V_S \approx 20$  mm/s. Examination of Fig. 9(A) reveals the origin of the discontinuity; the fast population reflects particles that are within the mLLDPE and the slow population reflects particles that are within the fluoropolymer layer. This is then a direct measurement of polymer–polymer slippage. The standard deviation in this graph has the same source and magnitude as discussed in Fig. 5.

In Fig. 9(B), we plot the velocity profiles for the five throughputs. All curves show this discontinuity at the wall, although for clarity we do not show the fluoropolymer data points at  $V_S \approx 0$ . Again, these curves are fits to Eq. (2). Figure 10 shows direct comparisons between the velocity profiles with and without the PPA. In each plot, the throughput, as set by the metering feeder, is the same. In each curve there is a crossover point, nearer the wall the velocity is greater with the PPA, whereas nearer the center the velocity is greater with no PPA. This is simply due to the conservation of mass.

In Fig. 11, we plot the velocity of the mLLDPE at the surface  $V(R) = V_S$  as a function of wall shear stress. In the case of the mLLDPE with the PPA system, we plot the velocity of the mLLDPE at the wall. The wall velocities in the presence of PPA range from approximately  $V_S \approx 7$  mm/s at low shear stress to  $V_S \approx 60$  mm/s at high shear stress. Note that the wall velocity in the case without PPA is approximately two orders

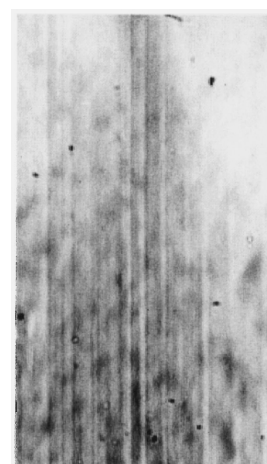


**FIG. 8. Micrograph of the polymer–polymer interface. The height of the micrograph corresponds to 200  $\mu\text{m}$ .**

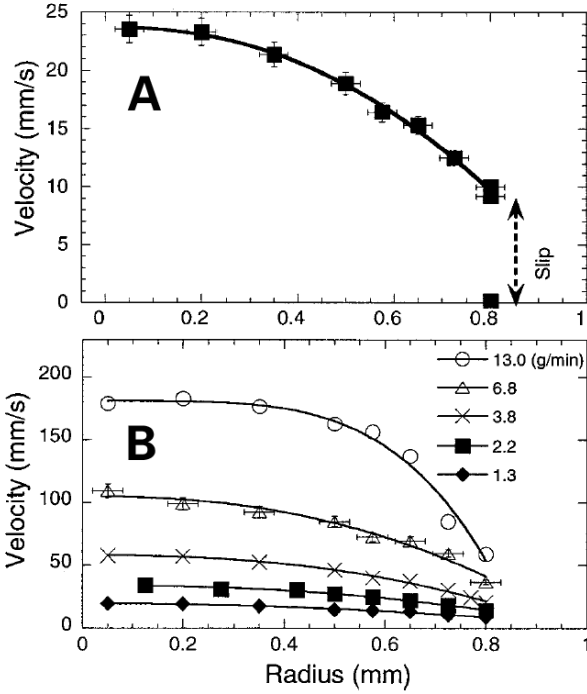


**FIG. 9. Velocity profiles with the addition of the PPA provide the first direct evidence of polymer–polymer slippage. (A)  $Q = 1.9$  g/min. Note the discontinuous jump in velocity in the immediate vicinity of the wall. (B) The five flow rates correspond to those in the lower curve of Fig. 3. All five curves show a similar discontinuous jump in velocity at the wall.**

of magnitude smaller. The standard deviation in the wall stress axis is due to pressure fluctuations and that in the velocity direction is smaller than the size of a data point. In Fig. 12, we plot the extrapolation length  $b = V_s / \dot{\gamma}_w$ , as a function of wall shear stress (see Fig. 1). In the case without PPA, the values of  $b$  are in the  $1 \mu\text{m}$  range. If one considers a particle right at the wall of radius  $e$ , and if there is a no-slip boundary condition, then one would find that  $b = e$ . As our microscope can see particles down to about  $1 \mu\text{m}$  radius, then the values of  $b$  that we obtain in the absence of PPA are the lowest that our system is capable of measuring and are fully consistent with a no-slip boundary condition. The standard deviation in  $b$  is due mainly to that in the value of  $\dot{\gamma}_w$ , which is based on the standard deviation from the fits of the velocity profiles. As noted above, Table I shows that the power-law index  $n$  is a decreasing function of increasing shear rate. We also note that for similar throughputs  $n$  is larger in the presence of PPA. This is consistent with the notion (to be quantified below) that the shear rate is reduced in the presence of the PPA.

In the presence of PPA, we obtain values of  $b$  in the  $100 \mu\text{m}$  range. Comparing these results to the theoretical models, we can gain an important insight into our system. Brochard and de Gennes predict that at low values of polymer–polymer slippage,

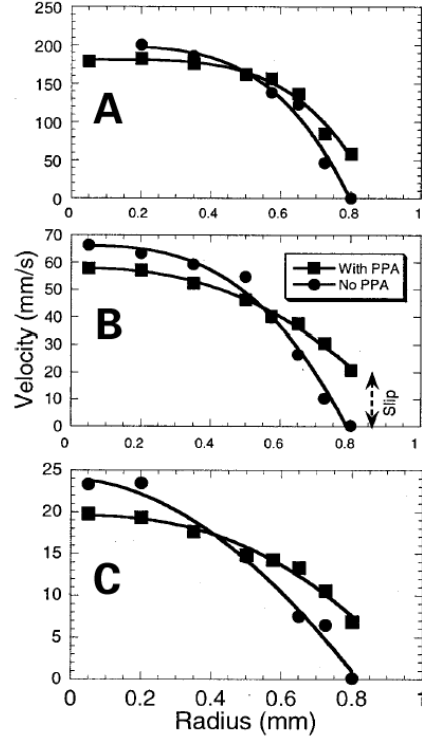


**FIG. 10. Direct comparison of flow profiles with and without PPA. (A)  $Q = 13.1$  g/min. (B)  $Q = 3.9$  g/min. (C)  $Q = 1.2$  g/min.**

the friction at the interface is relatively large, indicative of a modest level of entanglement at the interface. At larger values of the slippage the polymers become disentangled at the interface and the friction decreases strongly. According to this picture,<sup>6,7</sup> values this large can only be obtained if the interface between the two polymers is sharp and the fluoropolymer and the polyolefin are fully disentangled; there is virtually no interpenetration of one polymer into the other at the interface. Then, the friction between the two materials is Rouse type rather than driven by entanglements.

It is also useful to consider the dimensionless ratio  $b/R$ . For  $b/R \ll 1$ , the consequences of slippage on the rheological measurements are minimal. We anticipate that rheological measurements first show effects of slippage when  $b/R \approx 0.05$ . We see that in the case without PPA,  $b/R$  is of order  $10^{-3}$ , whereas with PPA,  $b/R$  is of order 0.2. Figure 12 thus quantifies an effect seen in the velocimetry plots; that the PPA induces slippage which has important rheological consequences.

Now we consider a central question: What causes sharkskin and why is it reduced by fluoropolymers? The velocimetry in the absence of PPA indicates that slip–stick behavior does not occur inside the die and thus does not cause sharkskin. Equally, we can rule out flow behavior further upstream, such as in the entrance region to the die. It has been suggested that wall shear rate is the crucial parameter in determining whether or not there is sharkskin. However, we show in Fig.13 that this is not the case. The two curves show the polyolefin shear rate at the wall as a function of throughput. Throughput is a useful parameter since it is the most easily controlled parameter in an industrial

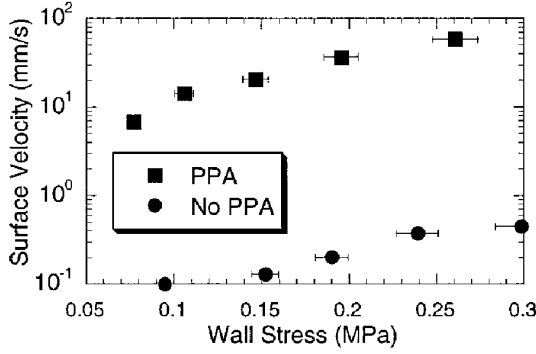


**FIG. 11. Velocity of surface particles as a function of wall shear stress for the cases with and without PPA. In the case with PPA, the surface velocity measures slippage whereas in the case without PPA, the low values are consistent with the no-slip boundary condition.**

process. First, we can see that for the same throughput, the shear rate is less in the case of added PPA. This difference persists for all five throughputs.

However, the reduction of shear rate upon addition of the PPAs is not the reason for the elimination of sharkskin. This can be seen upon comparison of the data points labeled (A)(no PPA) and (B)(with PPA). Sharkskin occurs only for the one with no PPA, even though its shear rate is approximately four times lower than in the case with PPA. Thus, wall shear is not the controlling parameter for sharkskin.

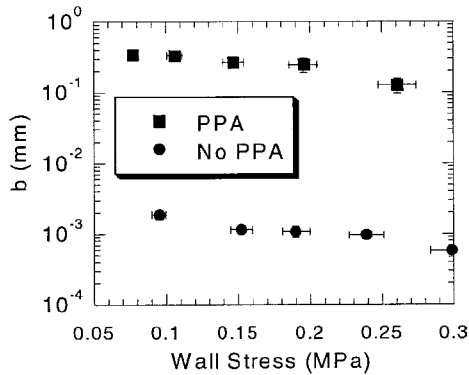


**FIG. 12. Extrapolation length ( $b$ ) as a function of wall shear stress for the cases with and without PPA.**

A promising explanation is found by considering the nature of the velocity rearrangements that occur as the mLLDPE transitions from the flow profile in the die to the uniform velocity profile that exists outside the die. Consider a thin finite layer of material of width  $\delta$  at the inside layer of the capillary tube, near the exit. Cogswell<sup>10</sup> discussed the extensional deformation that occurs in this layer of material; as it exits the tube its velocity increases until it reaches the final extrudate velocity:

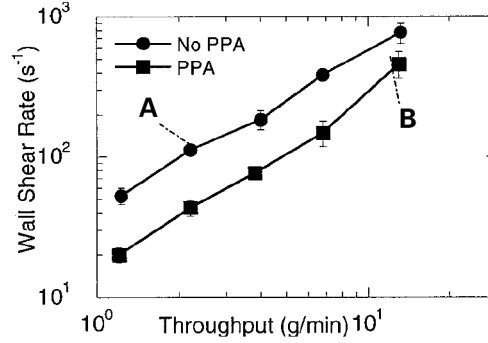


**FIG. 13. Wall shear rate as a function of throughput for the cases with and without PPA.**

$$V_f = Q / \pi R_f^2 \rho, \quad (3)$$

where  $R_f$  is the radius of the extrudate and  $\rho$  is the density. Concomitant with this increase in velocity is an increase in length and decrease in width. The total deformation of the layer is

$$T = V_f / V_\delta, \quad (4)$$

where  $V_\delta$  is the average velocity of the layer of material at a distance  $\delta$  from the die. Cogswell<sup>10</sup> utilized  $\delta = 50 \mu\text{m}$  because this corresponds to a sharkskin roughness level that would be visible to the eye. We use a smaller value consistent with what can be easily seen with a microscope ( $\delta = 20 \mu\text{m}$ ) while recognizing that this value is somewhat arbitrary. Figure 14 shows a plot of the  $V_f / V_\delta$  as a function of throughput for the cases with and without PPA. The largest source of error in this plot stems from the relative error in die swell measurements of 20%. The remarkable result is that the presence of slip causes a reduction in the total material deformation by an order of magnitude. The deformation is relatively insensitive to the total material throughput. Note that  $V_f / V_\delta$  does not take the rapidity of the deformation into account, nor does it assess the relative importance of viscous and elastic effects. Also, in the case of sharkskin,  $V_f / V_\delta$  is an “apparent deformation” because the true deformation is reduced by the sharkskin. This result gives new insight into how the polymer processing additives act.

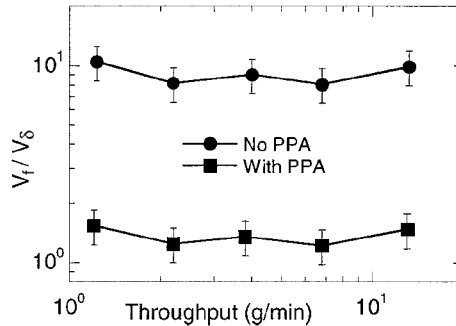


**FIG. 14. Total deformation of a thin layer at the surface of thickness  $\delta = 20 \mu\text{m}$  as it transitions from the capillary to the atmosphere.**

## CONCLUSION

The capillary rheo-optics methodology complements traditional capillary rheometry. By providing both flow velocimetry and high-speed imaging, a coherent picture of the suppression of sharkskin by use of fluoropolymer PPAs emerges. In the absence of the PPA, we confirm that slip in the die is not observed and thus is not a necessary ingredient for sharkskin. Upon addition of PPA, we observe the coating process through direct imaging. We see that the PPA forms elongated structures in the flow direction. The formation of the PPA layer coincides with the disappearance of the sharkskin in the extrudate.

Flow velocimetry in the presence of the PPA then shows that slip occurs for all throughputs. This slip is observed to occur at the interface between the two polymers. The magnitude of the slip extrapolation length (~200  $\mu\text{m}$ ) indicates that these two polymers are fully disentangled.

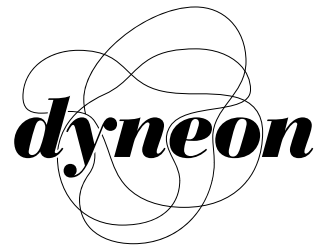
It is seen that the overall magnitude of the velocity rearrangements between the capillary die and the extrudate is greatly reduced upon addition of PPA. In particular, the total elongation in the surface layer is much reduced. More work is needed to quantify the extensional shear rate at the exit of the die.

While we use LLDPE on sapphire, the general results presented here are consistent with what one finds in a LLDPE/steel system. Specifically, sharkskin can occur on the bare surface beyond a threshold of approximately 0.1 MPa, but is reduced or eliminated upon the addition of a small quantity of a fluoropolymer added to the LLDPE. Thus, the PPA is able to coat both sapphire and steel. In the treated system, the effective viscosity is reduced, consistent with the drop in pressure that we measure.

For the range of temperatures and pressures investigated, we find that slippage of the LLDPE does not occur inside the sapphire capillary, even in the sharkskin regime. Typically, one uses a steel surface. Our experiments do not rule out the possibility that slippage can occur in the sharkskin regime on surfaces other than sapphire. If the Cogswell picture is the correct starting point, then the conditions at the exit determine the onset of sharkskin, rather than whether or not slippage in the tube occurs.

## REFERENCES

1. Ajdari, A., "Slippage at a polymer-polymer interface—Entanglements and Associated Friction," *C. R. Acad. Sci., Ser. II: Mec., Phys., Chim., Sci. Terre Univers* 317, 1159–1163 (1993).
2. Amos, S. E.; Giacoletto, G. M.; Horns, J. H.; Lavallée, C.; and Woods, S. S.; "Polymer processing additives (PPA)," in *Plastic Additives* Hanser, New York, 2001, pp. 553–584.
3. Barone, J. R.; Plucktaveesak, N., and Wang, S. Q., "Interfacial molecular instability mechanism for sharkskin phenomenon in capillary extrusion of linear polyethylenes," *J. Rheol.* 42, 813–832 (1998).
4. Barone, J. R.; Wang, S. Q., "Rheo-optical observations of sharkskin formation in slit-die extrusion," *J. Rheol.* 45, 49–60 (2001).
5. Brochard-Wyart, F., "Slippage at the interface between two slightly incompatible polymers," *C. R. Acad. Sci., Ser. II: Mec., Phys., Chim., Sci. Terre Univers* 310, 1169–1173 (1990).
6. Brochard-Wyart, F.; De Gennes, P. G. and Pincus, P.; "Suppression of sliding at the interface between incompatible polymer melts," *C. R. Acad. Sci., Ser. II: Mec., Phys., Chim., Sci. Terre Univers* 314, 873–878 (1992).
7. Brochard-Wyart, F. and De Gennes, P. G., "Sliding molecules at a polymer-polymer interface," *C. R. Acad. Sci., Ser. II: Mec., Phys., Chim., Sci. Terre Univers* 317, 13–17 (1993).
8. Brooks, R. V.; Briddell, J. E.; Fuller, R. L.; and Newman, K. E.; "Flow contamination tester," Eastman Chemical Company, U.S., Patent No. 5,790,249 (1998).
9. Chan, C. M. and Feng, J. Y., "Mechanisms for viscosity reduction of polymer blends: Blends of fluoroelastomer and high-density polyethylene," *J. Rheol.* 41, 319–333 (1997).
10. Cogswell, F. N., "Stretching flow instabilities at the exits of extrusion dies," *J. Non-Newtonian Fluid Mech.* 2, 37–47 (1977).
11. den Otter, J. L., "Mechanisms of melt fracture," *Plast. Polym.* 38, 155–168 (1970).
12. Denn, M. M., "Extrusion instabilities and wall slip," *Annu. Rev. Fluid Mech.* 33, 265–297 (2001).
13. Durliat, E., Hervet, H., and Leger, L., "Influence of grafting density on wall slip of a polymer melt on a polymer brush," *Europhys. Lett.* 38, 383–388 (1997).
14. El Kissi, N. and Piau, J. M., "Adhesion of linear low-density polyethylene for flow regimes with sharkskin," *Rheol. J.* 38, 1447–1463 (1994).
15. El Kissi, N.; Piau, J. M., and Toussaint, F.; "Sharkskin and cracking of polymer melt extrudates," *J. Non-Newtonian Fluid Mech.* 68, 271–290 (1997).
16. Ghanta, V. G., B. L. Riise, and M. M. Denn, "Disappearance of extrusion instabilities in brass capillary dies," *J. Rheol.* 43, 435–442 (1999).
17. Goveas, J. L. and Fredrickson, G. H., "Apparent slip at a polymer-polymer interface," *Eur. Phys. J. B* 2, 79–92 (1998).
18. Hatzikiriakos, S. G. and Dealy, J. M., "Wall slip of molten high-density polyethylene 1. Sliding plate rheometer studies," *Rheol. J.* 35, 497–523 (1991).
19. Hobbie, E. K. and Migler, K. B., "Vorticity elongation in polymeric emulsions," *Phys. Rev. Lett.* 82, 5393–5396 (1999).
20. Horns, J., "The influence of using fluoropolymer processing additives to improve the extrusion characteristics of LDPE/LLDPE resin blends," *SPE ANTEC Tech. Papers* 43, 64–69 (1997).
21. Howells, E. R. and Benbow, J. J.; "Flow defects in polymer melts," *Trans. Plast. Inst.* 30, 246–253 (1960).
22. Inn, Y. W.; Fischer, R. J., and Shaw, M. T., "Visual observation of development of sharkskin melt fracture in polybutadiene extrusion," *Rheol. Acta* 37, 573–582 (1998).
23. Inn, Y. W.; Wang, L. S., and Shaw, M. T., "Efforts to find stick-slip flow in the land of a die under sharkskin melt fracture conditions: Polybutadiene," *Macromol. Symp.* 158, 65–75 (2000).
24. Li, S., Migler, K. B.; Hobbie, E. K.; Kramer, H.; Han, C. C.; and Amis, E. J.; "Light-scattering photometer with optical microscope for the in-line study of polymer extrusion," *J. Polym. Sci., Part B: Polym. Phys.* 35, 2935–2943 (1997).



25. Lo, H. H. K.; Chan, C. M.; and Zhu, S. H.; "Characterization of the lubricant layer formed at the interface between the extrudate and the die wall during the extrusion of high-density polyethylene and fluoroelastomer blends by XPS, SIMS, and SEM," *Polym. Eng. Sci.* 39, 721-732 (1999).
26. Lyngaae-Jorgensen, J., "On the influence of interfacial slip on melt flow properties of polymer blends," *Int. Polym. Process.* 11, 123-130 (1988).
27. Mackley, M. R.; Rutgers, R. P. G.; and Gilbert, D. G., "Surface instabilities during the extrusion of linear low-density polyethylene," *J. Non-Newtonian Fluid Mech.* 76, 281-297 (1998).
28. Massey, G., Hervet, H. and Leger, L., "Investigation of the slip transition at the melt polymer interface," *Europhys. Lett.* 43, 83-88 (1998).
29. Migler, K. B., Hervet, H., and Leger, L., "Slip transition of a polymer melt under shear-stress," *Phys. Rev. Lett.* 70, 287-290 (1993).
30. Migler, K. B.; Gettinger, C. L.; Thalacker, V. P., and Conway, R., "Direct measurement of slippage induced by a polymer processing additive," *SPE ANTEC Tech. Papers* 45, 3128-3131 (1999).
31. Migler, K. B.; Hobbie, E. K. and Qiao, F., "In-line study of droplet deformation in polymer blends in channel flow," *Polym. Eng. Sci.* 39, 2282-2291 (1999b).
32. Munstedt, H., Schmidt, M., and Wassner, E., "Stick and slip phenomena during extrusion of polyethylene melts as investigated by laser-Doppler velocimetry," *J. Rheol.* 44, 413-428 (2000).
33. Nam, S., "Mechanism of fluoroelastomer processing aid in extrusion of LLDPE," *Int. Polym. Process.* 1, 98-101 (1987).
34. Piau, J. M., El Kissi, N., and Mezghani, A., "Slip-flow of polybutadiene through fluorinated dies," *J. Non-Newtonian Fluid Mech.* 59, 11-30 (1995).
35. Ramamurthy, A. V., "Wall slip in viscous fluids and influence of materials of construction," *J. Rheol.* 30, 337-357 (1986).
36. Tremblay, B., "Sharkskin defects of polymer melts—The role of cohesion and adhesion," *J. Rheol.* 35, 985-998 (1991).
37. Woods, S. S. and Amos, S. E., "The use of polymer processing additives to reduce gel formation in polyolefin plastomer extrusion," in *Proceedings of the TAPPI Laminations and Coatings Conference* (Tappi Press, 1998), pp. 675-685 (unpublished).

### Technical Information and Test Data

Technical information, test data, and advice provided by Dyneon personnel are based on information and tests we believe are reliable and are intended for persons with knowledge and technical skills sufficient to analyze test types and conditions, and to handle and use raw polymers and related compounding ingredients. No license under any Dyneon or third party intellectual rights is granted or implied by virtue of this information.

A 3M Company

### Important Notice:

Because conditions of product use are outside Dyneon's control and vary widely, user must evaluate and determine whether a Dyneon product will be suitable for user's intended application before using it. **The following is made in lieu of all express and implied warranties (including warranties of merchantability and fitness for a particular purpose): If a Dyneon product is proved to be defective, Dyneon's only obligation, and user's only remedy, will be, at Dyneon's option, to replace the quantity of product shown to be defective when user received it or to refund user's purchase price. In no event will Dyneon be liable for any direct, indirect, special, incidental, or consequential loss or damage, regardless of legal theory, such as breach of warranty or contract, negligence, or strict liability.**

© Dyneon 2001  
Issued: 10/01

Printed in USA  
98-0504-1326-3  
All Rights Reserved

### Product Information:

+1 651 733 5353 +1 800 723 9127

### Dyneon Sales Offices:

Dyneon LLC 6744 33rd Street North Oakdale, MN 55128 Phone: +1 651 733 5353 Fax: +1 651 737 7686 Toll Free: +1 800 723 9127	Dyneon GmbH & Co. KG Hammfelddamm 11 D-41460 Neuss, Germany Phone: +49 2131 14 2227 Fax: +49 2131 14 3857	Dyneon GmbH & Co. KG Werk Kelsterbach D-65444 Kelsterbach, Germany Phone: +49 6107 772 516 Fax: +49 6107 772 517	Dyneon N.V. Canadastraat 11, Haven 1005 B-2070 Zwijndrecht, Belgium Phone: +32 3 250 7537 Fax: +32 3 250 7905	Dyneon GmbH & Co. KG Succursale France Boulevard de l'Oise, Tour 3M F-95006 Cergy France Phone: +33 1 3031 6611 Fax: +33 1 3031 6613	Dyneon GmbH & Co. KG Sede Secondaria Italia Via San Bovio, 3 Milano San Felice I-20090 Segrate (MI) Italy Phone: +39 02 7035 3206-7 Fax: +39 2 7035 3208	Dyneon GmbH & Co. KG UK Branch House 3M House P.O. Box 1, Market Place Bracknell, Berkshire, RG121JU United Kingdom Phone: +44 1344 429675 Fax: +44 1344 427904	Sumitomo 3M Limited 33-1 Tamagawadai 2-chome Setagaya-Ku, Tokyo 158 Japan Phone: +81 03 3709 8111 Fax: +81 33709 8743	3M China Limited 10/F, New Town Mansion 55 Lou Shan Guan Road Shanghai 200335 P.R.C. Phone: +86 21 6275 3535 Fax: +86 21 6275 2343	3M Singapore Pte. Ltd. 9, Tagore Lane Singapore 787472 Phone: +65 450 8822 Fax: +65 552 2119	3M Australia Pty., Ltd. 950 Pacific Highway Pymble, N.S.W. 2073 Australia Phone: +61 2 9498 9333 Fax: +61 2 9498 9666	3M Canada Inc. P.O. Box 5757 London, Ontario NGA 4T1 Phone: +519 451 2500 Fax: +519 452 6262	3M Brazil Via Anhanguera, km, 110 Sumare, San Paulo CEP 13181-900 Phone: +55 19864 7000 Fax: +55 3838 6606
---	---	--	--	--	--	--	--	--	--	--	--	---

[www.dyneon.com](http://www.dyneon.com)

Dynamar and Dyneon are  
trademarks of Dyneon

**Warranty, Limited Remedy, and Disclaimer:** Many factors beyond 3M's control and uniquely within user's knowledge and control can affect the use and performance of a 3M product in a particular application. User is solely responsible for evaluating the 3M product and determining whether it is fit for a particular purpose and suitable for user's method of application. Unless a different warranty is specifically stated in the applicable product literature or packaging insert, 3M warrants that each 3M product meets the applicable 3M product specification at the time 3M ships the product. 3M MAKES NO OTHER WARRANTIES OR CONDITIONS, EXPRESS OR IMPLIED, INCLUDING, BUT NOT LIMITED TO, ANY IMPLIED WARRANTY OR CONDITION OF MERCHANTABILITY OR FITNESS FOR A PARTICULAR PURPOSE OR ANY IMPLIED WARRANTY OR CONDITION ARISING OUT OF A COURSE OF DEALING, CUSTOM OR USAGE OF TRADE. If the 3M product does not conform to this warranty, then the sole and exclusive remedy is, at 3M's option, replacement of the 3M product or refund of the purchase price.

**Limitation of Liability:** Except where prohibited by law, 3M will not be liable for any loss or damages arising from the 3M product, whether direct, indirect, special, incidental or consequential, regardless of the legal theory asserted, including warranty, contract, negligence or strict liability.

**Technical Information:** Technical information, recommendations, and other statements contained in this document or provided by 3M personnel are based on tests or experience that 3M believes are reliable, but the accuracy or completeness of such information is not guaranteed. Such information is intended for persons with knowledge and technical skills sufficient to assess and apply their own informed judgment to the information. No license under any 3M or third party intellectual property rights is granted or implied with this information.



3M Center  
St. Paul, MN 55144-1000  
1-800-810-8499  
[www.3M.com/fluoropolymers](http://www.3M.com/fluoropolymers)

Please recycle. Printed in USA.  
© 3M 2014. All rights reserved.  
98-0504-1326-3

3M is a trademark of 3M.  
Used under license.